Bioactive Materials 17 (2022) 457–470

Contents lists available at ScienceDirect

Bioactive Materials

journal homepage: www.keaipublishing.com/en/journals/bioactive-materials

Extracellular vesicles derived from neural EGFL-Like 1-modified mesenchymal stem cells improve acellular bone regeneration via the miR-25-5p-SMAD2 signaling axis

Yanhua Lan [a,1], Huizhi Xie [b,1], Qianrui Jin [a], Xiaomin Zhao [a], Yang Shi [a], Yanyan Zhou [a], Zihe Hu [a], Yi Ye [a], Xiaoyuan Huang [a], Yingjia Sun [a], Zhuo Chen [a,**], Zhijian Xie [a,*]

[a] Stomatology Hospital, School of Stomatology, Zhejiang University School of Medicine, Clinical Research Center for Oral Diseases of Zhejiang Province, Key Laboratory of Oral Biomedical Research of Zhejiang Province, Cancer Center of Zhejiang University, Hangzhou, 310006, China
[b] Department of Orthopaedics and Traumatology, Li Ka Shing Faculty of Medicine, The University of Hong Kong, Pokfulam, Hong Kong, 999077, China

ARTICLE INFO

Keywords:
Extracellular vesicles
Mesenchymal stem cells
Bone regeneration
Cell-free scaffolds
miRNAs

ABSTRACT

Stem cell based transplants effectively regenerate tissues; however, limitations such as immune rejection and teratoma formation prevent their application. Extracellular vesicles (EVs)-mediated acellular tissue regeneration is a promising alternative to stem cell based transplants. Although neural EGFL-like 1 (*Nell1*) is known to contribute to the osteogenic differentiation of bone marrow stem cells (BMSCs), it remains unknown whether EVs are involved in this process. Here, we present that EVs derived from *Nell1*-modified BMSCs (*Nell1*/EVs) have a stronger ability to promote BMSC osteogenesis owing to miR-25–5p downregulation. MiR-25–5p inhibits osteogenesis by targeting *Smad2* and suppressing the SMAD and extracellular signal-related kinase 1 and 2 (ERK1/2) pathway activation. In addition, we demonstrate that the 3D-*Nell1*/EV-hydrogel system is beneficial for bone regeneration *in vivo*, probably stemming from a slow, continuous release and high concentration of EVs in the bone defect area. Thus, our results have shown the potential of *Nell1*/EVs as a novel acellular bone regeneration strategy. Mechanistically, the identification of miR-25-5p-SMAD2 signaling axis expands the knowledge of *Nell1*/EVs induced osteogenesis.

1. Introduction

Bone defects can be caused by various clinical diseases and can severely limit rehabilitation [1,2]. However, repairing large bone defects remains a serious challenge [1,3]. Autografts, allografts, xenografts, and other approaches have been used to treat bone defects but clinical challenges such as tissue source, long surgical time, donor site morbidity [2], risk of disease transmission, and immunoreaction [4,5] have increased significantly. Recently, tissue engineering has been considered as a promising approach for bone regeneration that overcomes these difficulties by utilizing compatible biomaterials, growth factors, and cells [6,7]. Mesenchymal stem cells (MSCs) are multipotent cells with great potential for triggering bone healing after systemic/local infusion with cell-sheets/aggregates [8,9]. Furthermore, bone marrow stem cells (BMSCs), a critical category of MSCs, exhibit osteogenic properties [10,11]. However, their broader applications are severely limited by the low transplantation retention rate, immune rejection [12,13], teratoma formation [12], undirected cell differentiation [12,14], and pathological changes [15]. Numerous studies have shown that BMSCs exert therapeutic effects primarily through paracrine mechanisms [16–18]. To exploit this, acellular regeneration strategies utilizing the cell secretome, such as conditioned media (CM), soluble factors, and vesicular secretions, have been proposed along with the use of extracellular vesicle (EVs) as molecular propellers [19,20].

EVs are nanoparticles (30–200 nm) secreted by various cell types; they have been used in tissue regeneration because of advantages over previous delivery mediators [18,21,22]. The lipid bilayer of EVs can retain their bioactivity for a long time and protect various functional

Peer review under responsibility of KeAi Communications Co., Ltd.
* Corresponding author.
** Corresponding author.
E-mail addresses: zoechen@zju.edu.cn (Z. Chen), xzj66@zju.edu.cn (Z. Xie).
[1] These authors contributed equally to the work and are thus co-first authors.

https://doi.org/10.1016/j.bioactmat.2022.01.019
Received 21 July 2021; Received in revised form 9 January 2022; Accepted 12 January 2022
Available online 19 January 2022

molecules, such as microRNAs (miRNAs) [22–25]. More importantly, EVs can be sterilized through filters, easily stored at −80 °C, utilized directly upon thawing, and lyophilized as off-the-shelf products [26,27]. Recently, basic preclinical studies have focused on the use of engineered EV therapies, while EV modification is gaining increasing attention in clinical studies [28–31]. One of the primary methods for MSC-EV modification/engineering is gene modification of parental cells before EV isolation (e.g., preconditioning or transfection/transduction of MSCs) [29,32]. Proper gene modification of EVs can significantly improve cellular uptake or therapeutic RNA delivery to promote the therapeutic efficacy of EVs beyond their native function [33]. Studies have suggested that gene-modified MSCs-EVs could promote bone regeneration and treat bone-related diseases [34]. EVs secreted from bone morphogenetic protein 2 (BMP2) overexpressed MSCs enhanced critical bone defect healing via its miRNA components [35]. The hypoxia-inducible factor 1α-overexpressed MSCs secrete EVs, which accelerates the bone recovery through angiogenesis [36]. EVs derived from BMSCs overexpressing glycoprotein non-melanoma clone B attenuates bone loss in an ovariectomized rat model [37]. Increasing evidence has shown that binding to or encasing EVs in a biomaterial matrix can prolong EVs bioavailability following delivery, achieve EVs sustained and controlled release, maintain the stability of EV cargo, and potentially augment therapeutic potency [19,38,39]. Recently, the development of biomaterials enriched with EVs has achieved promising results in promoting tissue regeneration, especially in localized diseases such as bone defects [40,41]. However, therapeutic strategies utilizing biomaterials encapsulating gene-modified BMSC-EVs and biomaterials with modified BMSC-EVs, particularly for improving the bone repair process, are lacking.

Neural EGFL-like 1 (NELL1) is a protein that stimulates bone formation and performs better than BMP2 in terms of its antiadipogenic, anti-inflammatory, and vascularization characteristics. *Nell1* has demonstrated efficacy in bone regeneration for systemic and local osteogenic treatments in various preclinical animal models [42–44]. In addition, *Nell1* significantly activates various pathways, including the mitogen activated protein kinase (MAPK) pathway, Wnt/β-catenin pathway, and Indian hedgehog pathway, all of which are involved in regulating osteogenesis [45]. Indeed, *Nell1* may be a suitable alternative gene for EV modification, specifically for bone regeneration.

We hypothesized that *Nell1* modification could induce a series of changes in BMSCs as well as EVs. Based on the results of our previous study, which verified the osteo-inductive capacity of BMSC-EVs on the titanium surface of dental implants [46], we examined whether EVs secreted from *Nell1*-modified BMSCs (*Nell1*/EVs) could induce osteogenesis *in vitro* and acellular bone regeneration *in vivo* (Fig. 1). Indeed, *Nell1*/EVs showed favorable osteogenic capability involving the miR-25-5p-SMAD2 signaling axis. Meanwhile, 3D-EV-hydrogel with *Nell1*/EVs was used to achieve acellular bone regeneration. Taken together, the acellular regeneration method based on *Nell1*/EVs is a promising strategy for bone defect healing. A key mechanism in this process is the altered fate-modifying EV-miRNAs and miRNA-target gene regulatory network, which improves the understanding of the osteo-inductive effect of *Nell1*.

2. Materials and methods

All methods can be found in the accompanying Supplemental Information file II.

3. Results

3.1. *Nell1/EVs are essential component of Nell1/CM in promoting osteogenic differentiation*

Rat BMSCs were identified based on their morphology (Fig. S1A) and flow cytometric analysis (Fig. S1B). Primary cells exhibited a typical spindle shape for single BMSCs and a whirlpool-like arrangement for BMSC colonies. The phenotypic characterization of BMSCs was confirmed by positive staining for CD29 and CD90 and negative staining for CD34 and CD45. Next, *Nell1*-modified BMSCs (*Nell1*/BMSCs) were obtained by transfection of full-length *Nell1*; after 48 h of transfection, more than 50% of the cells were positive for GFP (Fig. 2A). BMSCs transfected with negative lentivirus (*Ctrl*/BMSCs) were used as negative controls. As shown in Fig. 2B–D, *Nell1* protein and mRNA expression were much higher in *Nell1*/BMSCs than *Ctrl*/BMSCs.

As shown in Fig. 2E–G, *Nell1*/CM induced robust osteogenic differentiation of BMSCs on days 7 and 14 based on an enhanced alkaline phosphatase (ALP) expression and calcium deposition. As such, a classical EV blocker (GW4869) was employed to investigate whether EVs play a key role in this pro-osteogenic effect. Quantification of EVs protein content was quantified, and the results suggested that GW4869 reduced the number of EVs acquired via ultracentrifugation by ~50%

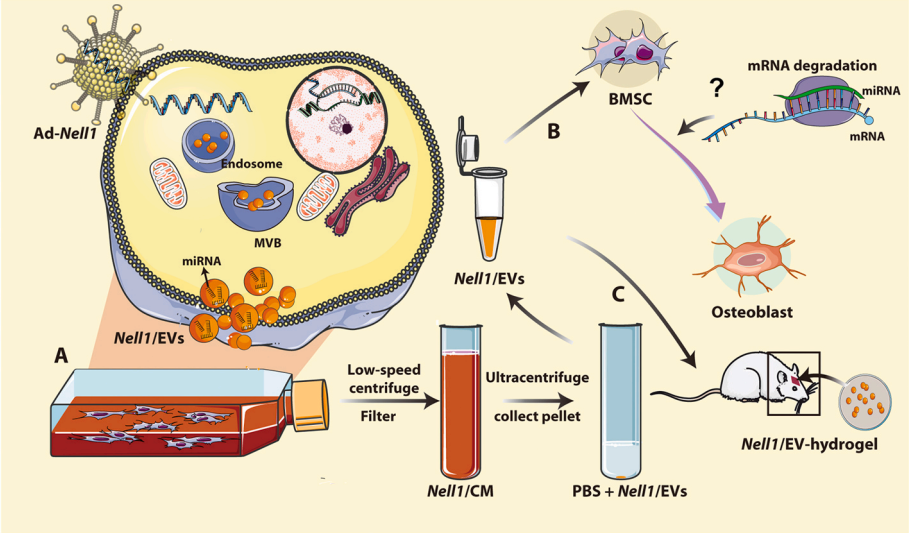

Fig. 1. Acellular bone tissue regeneration by *Nell1*-modified-EVs (*Nell1*/EVs). **(A)** *Nell1*/EVs were isolated from *Nell1*-modified-BMSCs. **(B)** *In vitro* studies of the induction and mechanism of action of *Nell1*/EVs regulatory BMSC osteogensis. **(C)** *In vivo*, calvarial defects were used as animal models to evaluate the bone defect repair capacity of 3D-*Nell1*/EV-hydrogel. *Nell1*/EVs and negative control EVs were encased in the hydrogel for further implantation in defects.

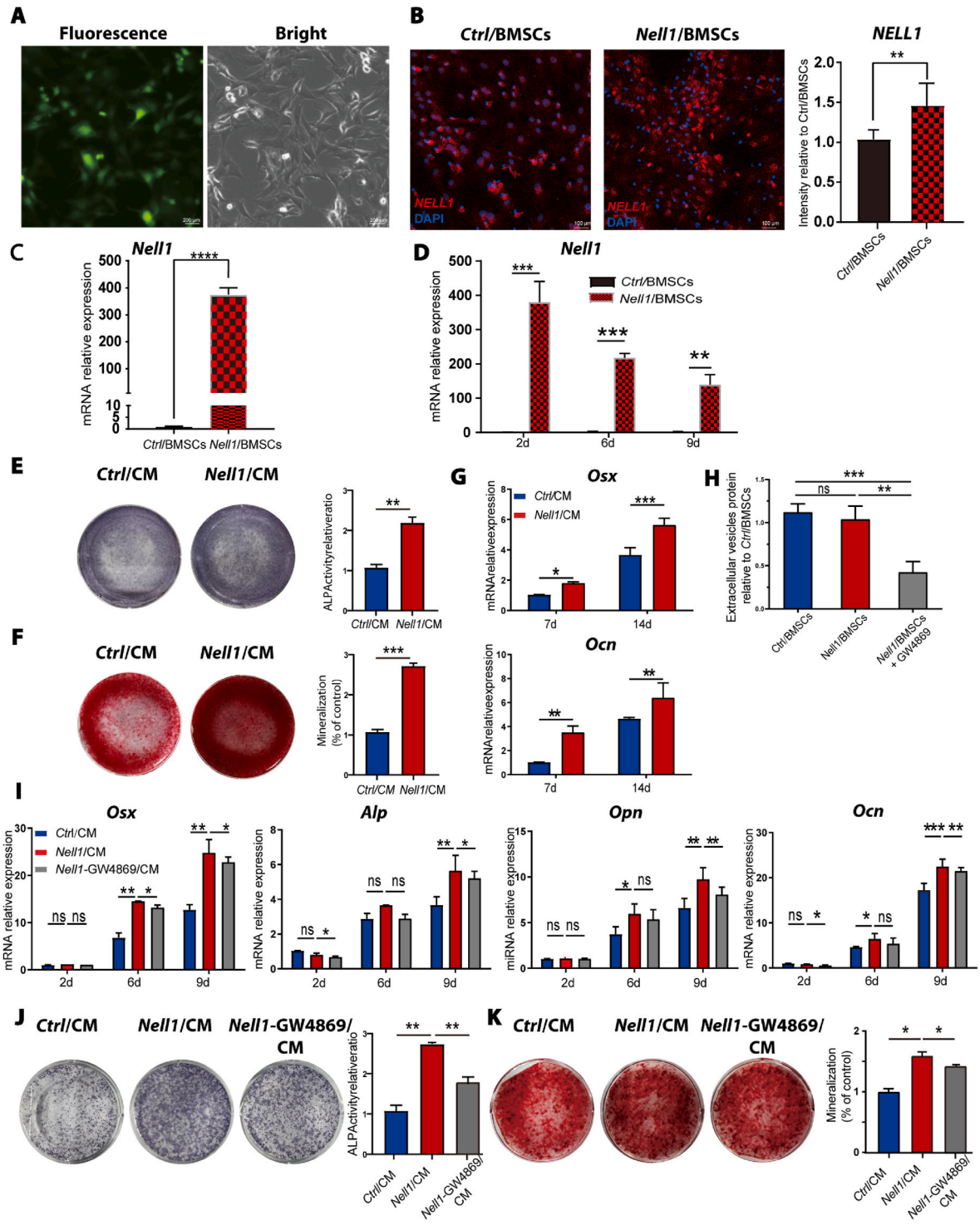

Fig. 2. Osteogenic differentiation capacity of conditioned media from *Nell1*/BMSCs (*Nell1*/CM) depends on EVs. **(A)** Representative images of *Nell1*-green fluorescent protein (GFP) adenovirus (Ad-*Nell1*) infection in BMSCs *in vitro*. **(B)** Immunofluorescence-based detection of NELL1. **(C)** Determination of *Nell1* overexpression in BMSCs by RT-qPCR. **(D)** RT-qPCR analysis of *Nell1* transcription in BMSCs infected with Ad-*Nell1* at day 2, 6, and 9. **(E)** Alkaline phosphatase (ALP) staining and quantitative ALP assay of BMSCs incubated with *Nell1*/CM or *Ctrl*/CM for 7 days. **(F)** Alizarin red staining and semi-quantitative analysis of BMSCs incubated with *Nell1*/CM or *Ctrl*/CM for 14 days. **(G)** RT-qPCR determination of osteogenic markers expression on day 7 and 14. **(H)** Quantification of EV protein content. EVs were collected from the conditioned media of each group: *Ctrl*/BMSCs, *Nell1*/BMSCs treated with or without GW4869. **(I)** Mineralization induction in fresh osteoinductive medium with *Nell1*/CM, *Ctrl*/CM, or *Nell1*-GW4869/CM. RT-qPCR determination of osteogenic marker expression on day 2, 6, and 9. **(J)** In co-incubation mineralization experiments, ALP staining and quantitative ALP assay at day 14. **(K)** Alizarin red staining of BMSCs and semi-quantification at day 21. *p < 0.05, **p < 0.01, ***p < 0.001, NS, non-significant, via *t*-test or one-way analysis of variance, n = 3. CM, conditioned media.

(Fig. 2H) compared with *Nell1*/BMSCs. Interestingly, the mRNA expression of osteogenic markers, including *Osterix (Osx)*, *Alp*, *Osteopontin (Opn)*, and Osteocalcin (*Ocn)*, was substantially increased in the *Nell1*/CM group; however, it decreased when EV production was inhibited (Fig. 2I). Consistently, the increased ALP expression (Fig. 2J) and mineralization capability (Fig. 2K) in the *Nell1*/CM groups were reduced when EV production was inhibited. Together, these results suggested that *Nell1*/EVs are essential component of *Nell1*/CM in promoting osteogenic differentiation.

3.2. Characterization and pro-osteogenic ability of Nell1/EVs

To further evaluate the role of EVs in osteogenic differentiation, *Nell1*/EVs and *Ctrl*/EVs were isolated from *Nell1*/CM and *Ctrl*/CM using ultracentrifugation [47]. Before isolating EVs, we demonstrated that the viability of *Nell1*/BMSCs and *Ctrl*/BMSCs was over 98% at the time of EV harvest (Fig. S2). Transmission electron microscopy analysis suggested the presence of 50–200 nm particles that were morphologically consistent with EVs (Fig. 3A). Analysis with a NanosightNS300 revealed that particles isolated from *Ctrl*/CM and *Nell1*/CM had mean diameters of 153.0 ± 38.5 nm and 136.0 ± 31.5 nm, respectively (Fig. 3B). Particles isolated by ultracentrifugation expressed EV-specific markers (Alix, CD54, Flotillin-1, and Annexin V); however, they did not express GM130, a Golgi matrix protein (Fig. 3C). These results suggested that *Nell1*/EVs and *Ctrl*/EVs were successfully isolated with high purity. The results of the western blotting (WB) analysis demonstrated that the expression of NELL1 was significantly higher in *Nell1*/BMSCs than in *Ctrl*/BMSCs; however, there was no noticeable difference in NELL1 expression between *Nell1*/EVs and *Ctrl*/EVs. In both the EVs, NELL1 protein expression was extremely low (Fig. 3C).

We also examined whether *Nell1*/EVs could enhance the osteogenic potential of BMSCs *in vivo*. Significantly higher expression levels of *Runx2*, *Bmp2*, *Ocn*, and *Opn* were observed in *Nell1*/EVs on days 3 and 6 as compared with those in the phosphate-buffered saline (PBS) and *Ctrl*/

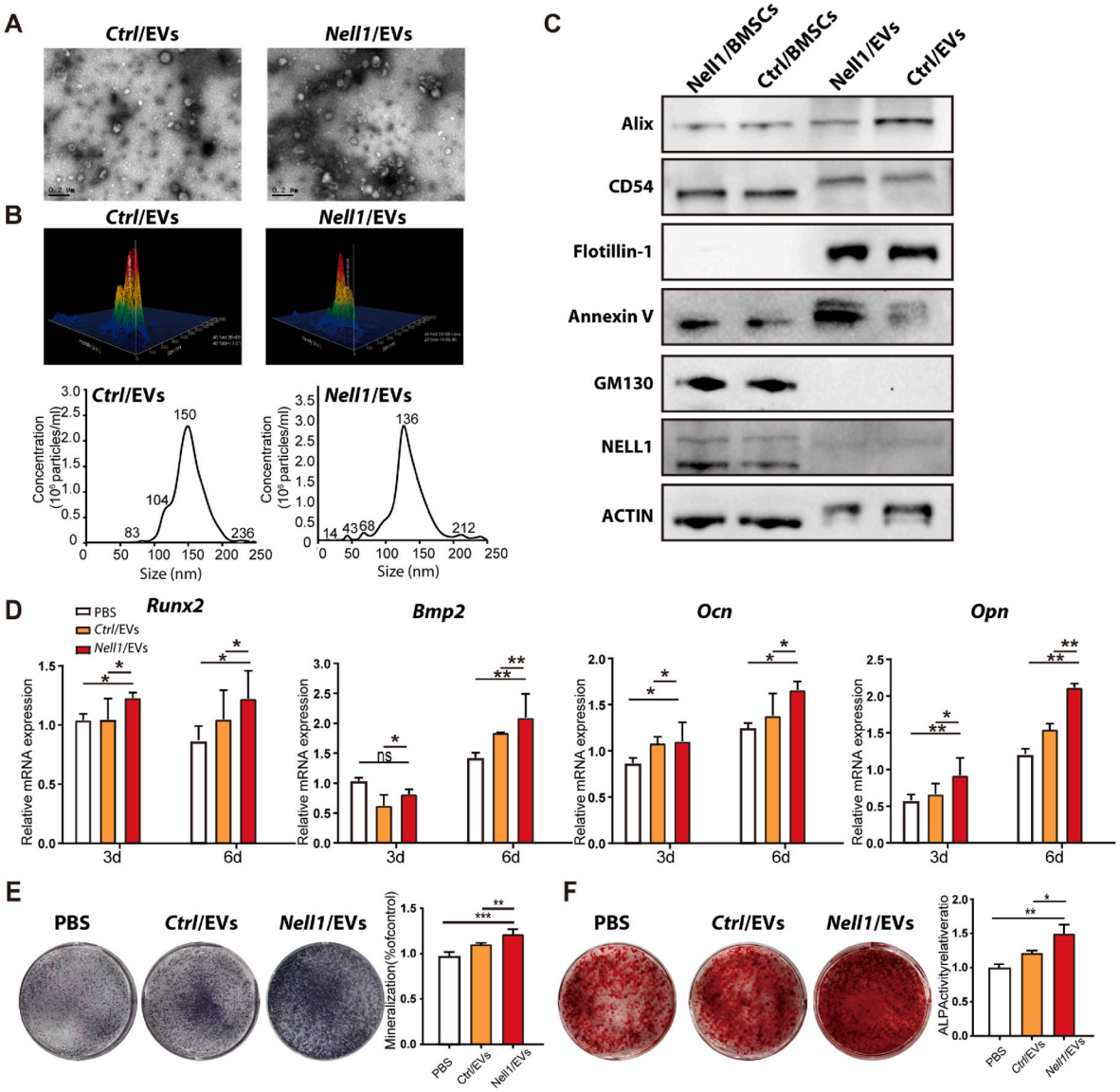

Fig. 3. Characterization and pro-osteogenic ability of *Nell1*-modified-EVs (*Nell1*/EVs). **(A)** Representative transmission electron microscopy images of the ultrastructure of *Nell1*/EVs and *Ctrl*/EVs. Scale bars: 200 nm. **(B)** Nanoparticle transport analysis of the size distribution and particle concentration of the two types of EVs. **(C)** Representative immunoblots showing expression of Alix, CD54, Flotillin-1, Annexin V and NELL1. GM130 was used here as a negative marker and ACTIN as a loading control. **(D)** RT-qPCR analysis of osteoblast gene markers in BMSCs treated with PBS, *Nell1*/EVs, or *Ctrl*/EVs at 3 and 6 days. **(E)** ALP staining images and ALP activity in BMSCs treated with PBS, *Nell1*/EVs, or *Ctrl*/EVs on day 14. **(F)** Alizarin Red-stained images and semi-quantification of BMSCs treated with PBS, *Nell1*/EVs, or *Ctrl*/EVs at day 21. *p < 0.05, **p < 0.01, ***p < 0.001, NS, non-significant, via *t*-test or one-way analysis of variance, n = 3.

EV groups (Fig. 3D). Correspondingly, ALP activity and calcium deposits in the *Nell1*/EV group at days 14 and 21 were increased compared to those in the PBS and *Ctrl*/EV groups (Fig. 3E and F). These results demonstrated that *Nell1*/EVs function as molecular propellers to modulate the osteogenic differentiation of BMSCs.

To investigate the mode of *Nell1*/EVs interaction mode and determine whether *Nell1*/EV and BMSCs communication is surface binding dependent, fluorescence-labeled EVs and BMSCs were cocultured at 4 °C and 37 °C, respectively (Fig. 4A). As shown in Fig. 4B, confocal fluorescence microscopy revealed hardly any *Nell1*/EVs (or *Ctrl*/EVs) were seen on BMSCs surface when coculture at 4 °C. However, the colocalization of BMSCs and *Nell1*/EVs (or *Ctrl*/EVs) was evident after 30 min of coculture at 37 °C. When the coculture time was extended to 5 h, there was also no significant colocalization of cells and EVs (Fig. S3). After coculture at 37 °C for 12 h, confocal fluorescence microscopy revealed that 80–90% of the BMSCs showed colocalization with EVs; there was no

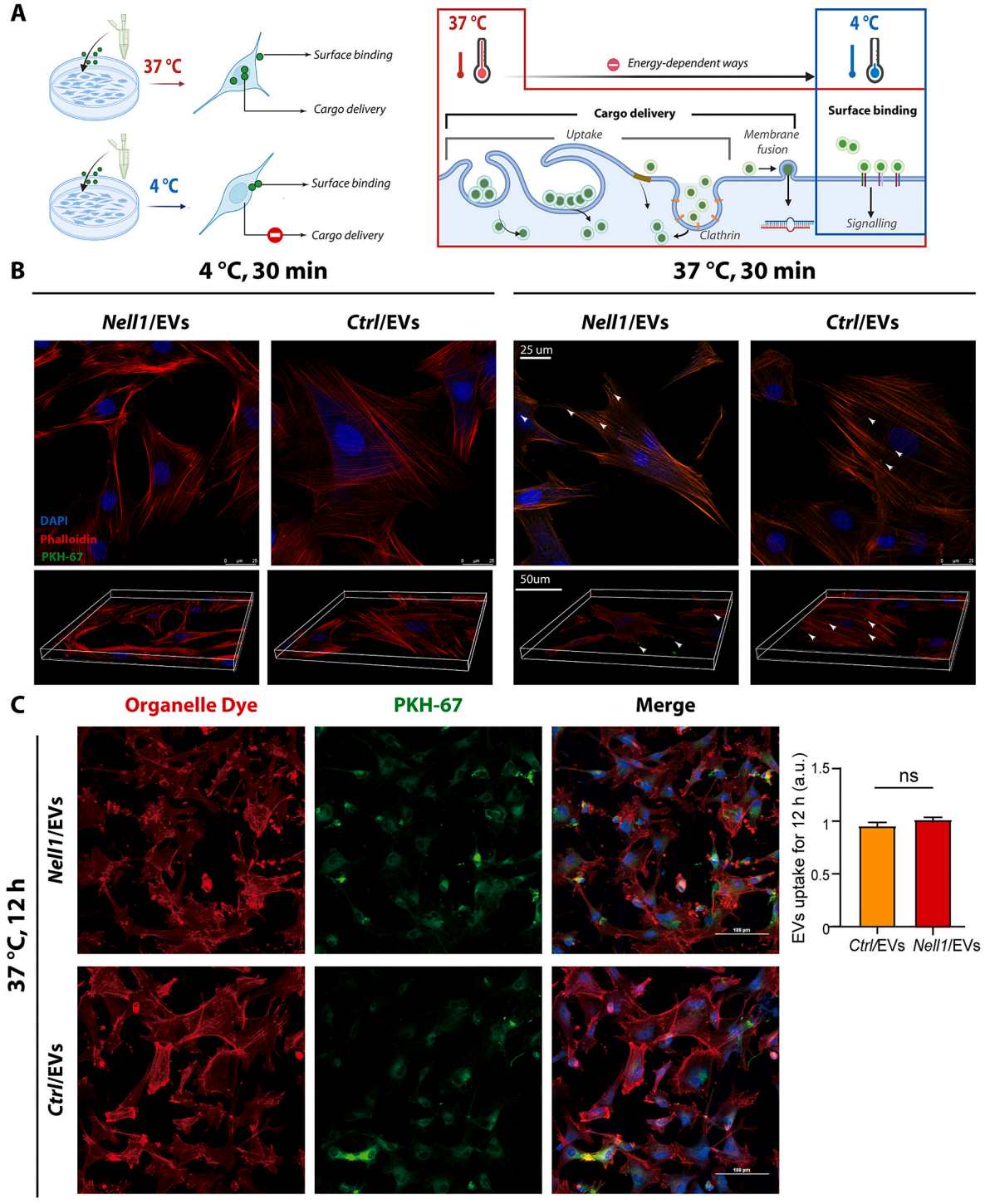

Fig. 4. *Nell1*/EVs interact with recipient cells in a surface binding-independent manner. (A) Experimental set-up to examine the mode of *Nell1*/EV interaction with target BMSCs. Schematic picture was created with BioRender. **(B)** BMSCs were cocultured with an equivalent amount of *Nell1*/EVs or *Ctrl*/EVs (10 μg/ml), incubated for 30 min under two temperature conditions: 4 °C and 37 °C. Z-stacks were observed by confocal microscopy. White arrows indicate *Ctrl*/EVs or *Nell1*/EVs. **(C)** Two types of EVs were taken up by BMSCs for 12 h at 37 °C. NS, non-significant, via *t*-test, n = 3.

significant difference between *Nell1*/EVs and *Ctrl*/EVs (Fig. 4C). These findings suggested that the *Nell1*/EVs-BMSCs interaction was in a surface binding-independent manner, and internalization (cargo delivery) of *Nell1*/EVs is more likely necessary for their pro-osteogenic effect.

3.3. Identification of differentially expressed miRNAs using high-throughput sequencing

Since miRNAs are key regulators of bone development, regeneration, and function [48–50]; EVs are the main route by which small RNA species are transferred between cells [24,47,51]. Moreover, we demonstrated previously that the cargos of *Nell1*/EVs are dominant to contribute to their osteogenic capacity. High-throughput sequencing was applied to investigate the role of miRNAs in *Nell1*/EV-induced osteogenic differentiation, and the results revealed differentially expressed miRNAs (DEMs) between *Nell1*/EV and *Ctrl*/EV groups. The heatmap showed the top 20 genes with the most significant differential expression (Fig. 5A). A scatterplot of Gene Ontology (GO) annotations showed the top 9 most enriched GO-biological process (BP) annotations of these DEMs (Fig. 5B); here, the TGF-β pathway was the most enriched, suggesting that it could play regulatory functions in *Nell1*/EV-induced bone formation. Kyoto Encyclopedia of Genes and Genomics (KEGG) enrichment analysis was performed to reveal pathways that were most significantly related to *Nell1*/EVs. Among these pathways several osteogenic differentiation-related processes were worth noting, such as aging, ERK1 and ERK2 cascade, angiogenesis, BMP signaling pathway,

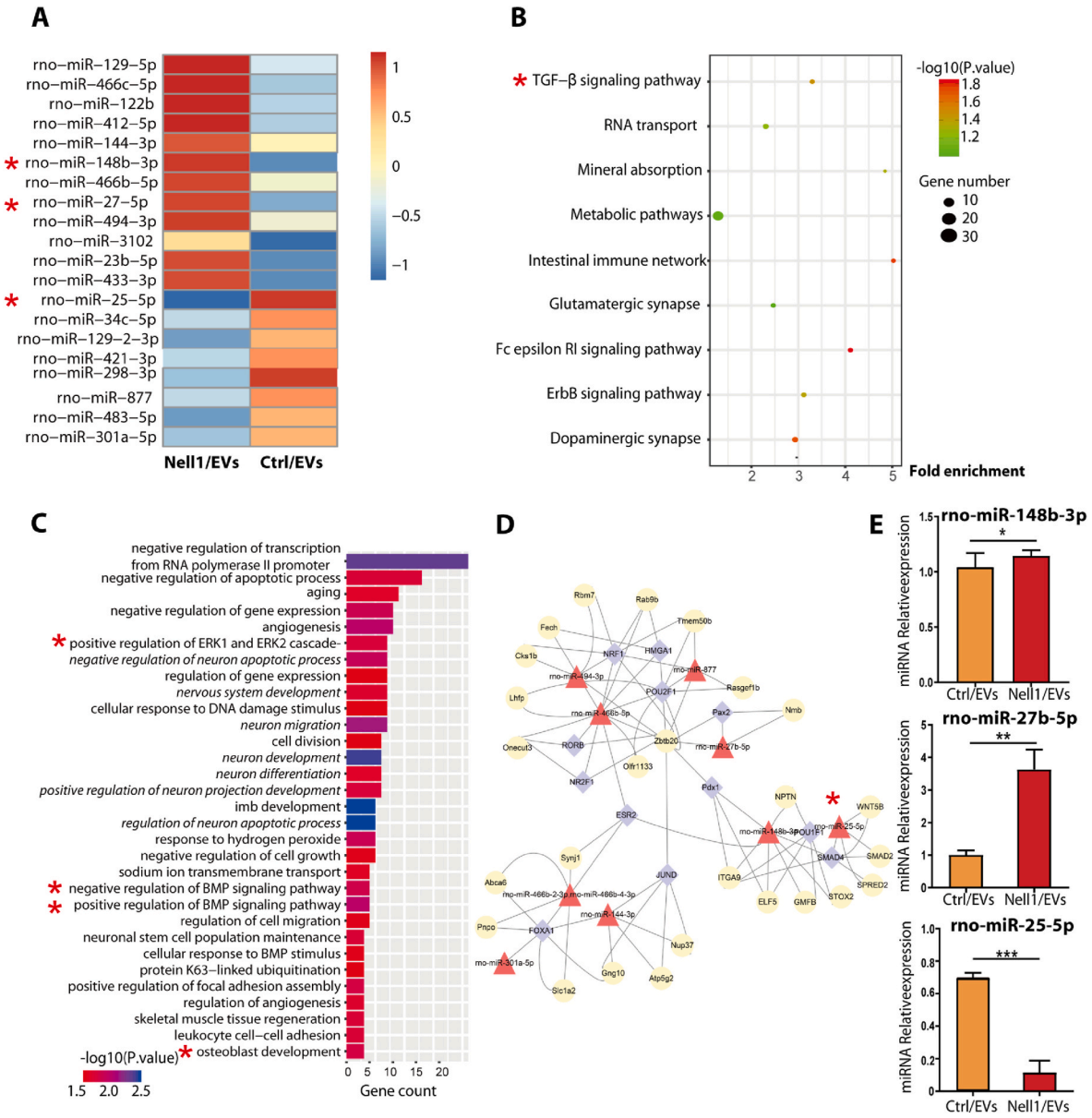

Fig. 5. Differentially expressed miRNAs profile in *Nell1*-modified-EVs (*Nell1*/EVs) and negative control EVs (*Ctrl*/EVs) were determined by miRNA sequencing. **(A)** Heatmap depicting the expression of differentially expressed miRNAs (DEMs) in *Nell1*/EVs or *Ctrl*/EVs. The top 20 miRNAs with the highest fold-change were identified. **(B)** Scatterplot of GO annotations. The top nine significant GO-BP annotations of the target genes of the DEMs are shown. The correlation between miRNA and related biological processes was measured using the negative $\log^{10}$ of the *p*-value. GO, Gene Ontology; BP, biological processes. **(C)** KEGG enrichment analysis. The top 31 most relevant KEGG pathways of the DEMs. KEGG, Kyoto Encyclopedia of Genes and Genomes. **(D)** Potential coregulatory network of miRNAs, TFs, and target genes. Diamonds, TFs; triangles, miRNAs; circles, genes. **(E)** RNA-Seq results of rno-miR-148b-3p, rno-miR-27b-5p, and rno-miR-25–5p validated by qRT-PCR. *$p < 0.05$, **$p < 0.01$, ***$p < 0.001$, via *t*-test, n = 3. * Colors indicate those chosen as the focus of this study. Osteogenic-related signaling pathways are shown in bold font; pathways related to neurodevelopment are marked in italics.

and osteoblast development (bold in Fig. 5C). In addition, several neurodevelopmental-related pathways were identified (italics in Fig. 5C). The network of miRNAs regulating critical genes was shown in Fig. 5D. The key regulatory positions of the 9 miRNAs are indicated. In conjunction with the heatmap data, the expression of rno-miR-148b-3p, rno-miR-27b-5p, and rno-miR-25–5p was further validated by reverse transcription-quantitative polymerase chain reaction (RT-qPCR) and bioinformatics analysis (Fig. S4). Rno-miR-25–5p exhibited the most pronounced changes (Fig. 5E), whereas the miR-25–5p level in EVs was reduced in response to *Nell1* modification.

3.4. *miR-25–5p suppressed osteogenic differentiation by directly targeting SMAD2*

We further investigated the potential mechanism of miR-25–5p in osteogenic differentiation. BMSCs were transfected with different miRNAs (miR-25–5p mimics and miR-25–5p inhibitors) and corresponding controls (negative control (miR-NC) and inhibitor negative control (anti-miR-NC)). Intracellular miR-25–5p was markedly upregulated in cells transfected with miR-25–5p mimics and markedly downregulated in cells transfected with miR-25–5p inhibitors, as compared to that in the corresponding controls (Fig. 6A). The proliferation of BMSCs was significantly increased after treatment with miR-25–5p inhibitors. In contrast, when miR-25–5p was overexpressed, BMSCs showed decreased proliferation ability, particularly at later time points (Fig. 6B). These results indicated the suppression of miR-25–5p promoted BMSCs proliferation *in vitro*. Functionally, the results showed that miR-25–5p inhibitors upregulated the expression of osteogenesis-related genes such as *Alp* and *Ocn*; however, miR-25–5p mimics downregulated these genes (Fig. 6C). Furthermore, miR-25–5p overexpression reduced ALP staining and mineralized nodule staining. In contrast, knockdown of miR-25–5p had the opposite effects (Fig. 6D and E). These results showed that miR-25–5p significantly inhibited the proliferation and differentiation of BMSCs toward the osteogenic lineage.

Bioinformatic analysis showed that *SMAD2* is a potential target of miR-25–5p, with a top-ranked predictive score. Western blotting revealed that SMAD2 expression was decreased by miR-25–5p mimics and increased by miR-25–5p inhibitors (Fig. 6F). The same trend was observed for the expression of *Smad2* mRNA (Fig. 6G). Additionally, 3'-untranslated region (UTR) luciferase reporter constructs containing wild-type (WT *Smad2* 3'-UTR reporter) and mutant (MUT *Smad2* 3'-UTR reporter) sequences of the miR-25–5p binding sites in the *Smad2* locus (Fig. 6H) were constructed. Co-transfection of BMSCs with the miR-25–5p mimics and luciferase plasmid confirmed that miR-25–5p

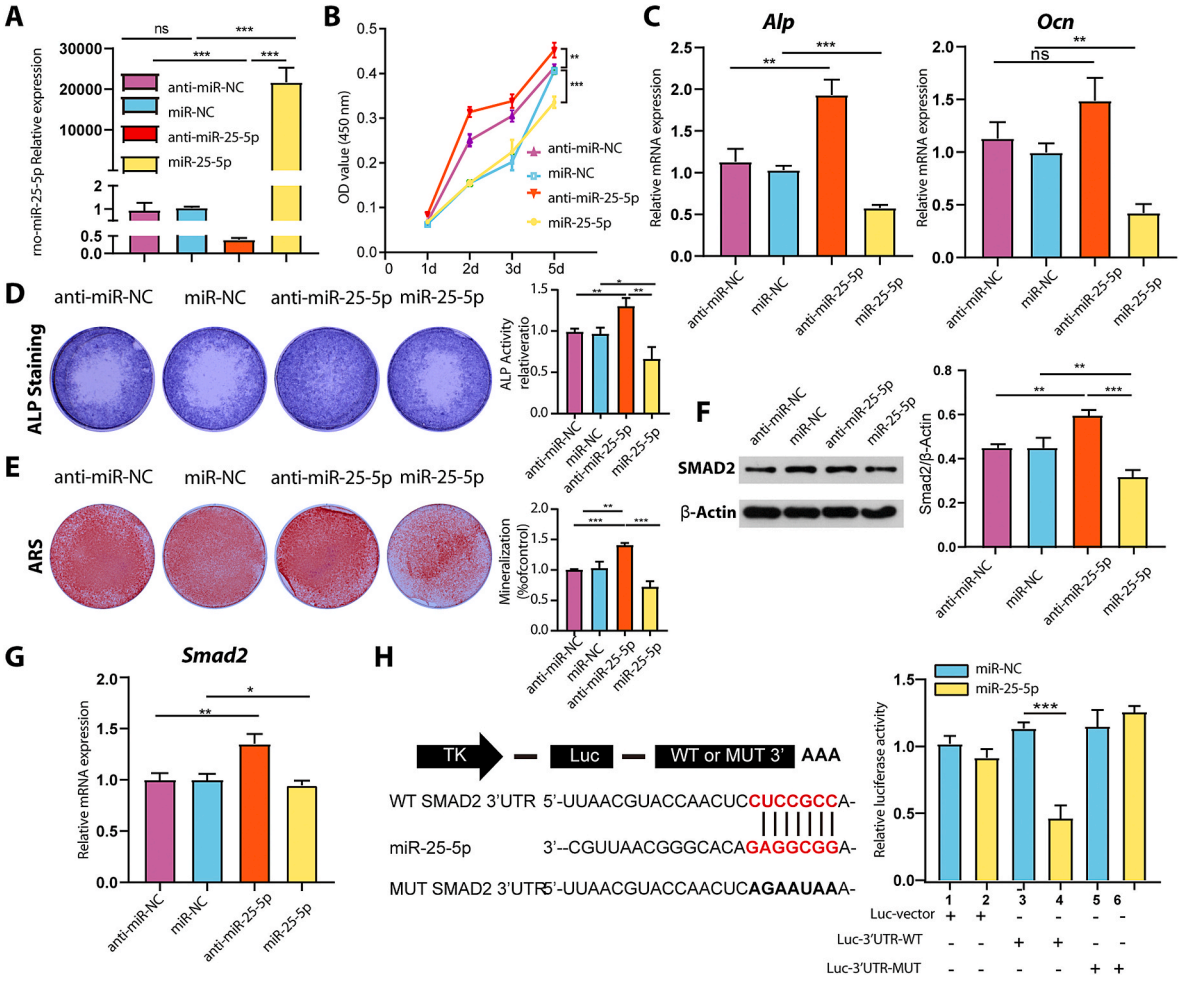

Fig. 6. Downregulation of miR-25-5p promoted osteogenic differentiation of BMSCs by directly targeting *Smad2*. (A) Expression levels of miR-25–5p were validated by RT-qPCR after transfection with miR-25–5p mimics or inhibitors. **(B)** Effect of miR-25–5p on BMSCs proliferation was measured using CCK-8 assays. **(C)** RT-qPCR was used to determine the expression of osteogenic markers (*Alp* and *Ocn*) after miRNA transfection. **(D)** ALP staining of BMSCs transfected with different miRNAs for 14 days. **(E)** Alizarin red staining of BMSCs treated with different miRNAs for 21 days. The effect of miR-25–5p on the expression of SMAD2 in BMSCs was assessed by **(F)** western blotting and **(G)** qRT-PCR **(H)** Luciferase reporter assay of the association between miR-25–5p and *Smad2*. MiR-25–5p, miR-25–5p mimics; anti-miR-25–5p, miR-25–5p inhibitors; miR-NC, mimic negative control; anti-miR-NC, inhibitor negative control. One-way analysis of variance was used. *p < 0.05, **p < 0.01, ***p < 0.001, NS, non-significant, n = 3.

specifically binds to the predicted target region in *Smad2* mRNA. The luciferase reporter activity of the WT *Smad2* 3'-UTR was significantly reduced after transfection with the miR-25–5p mimics; however, this was not observed in MUT *Smad2* 3′-UTR. These results indicated that miR-25–5p directly targets *Smad2* and binds to its 3'-UTR.

3.5. miR-25–5p/SMAD2/ERK as the critical mechanistic link for the osteogenic capacity of Nell1/EVs

The expressions of SMAD2 and *p*-SMAD2 were increased by miR-25–5p inhibitors and decreased by miR-25–5p mimics, as compared with those of the internal reference protein (Fig. 7A). Although the ratio of phosphorylated SMAD2 (*p*-SMAD2/SMAD2) was not altered by miR-25–5p mimics, the total amount of phosphorylated SMAD2 (*p*-SMAD2/β-actin) was significantly downregulated. Moreover, transfection with the miR-25–5p mimics inhibited the phosphorylation of extracellular signal-related kinase 1 and 2 (ERK1/2) in BMSCs (Fig. 7B). Further, immunofluorescence revealed that miR-25–5p mimics decreased the expressions of *p*-SMAD2 and *p*-ERK1/2, which indicated the inhibition of SMAD and ERK pathways (Fig. 7C and D). Collectively, these results verified that miR-25–5p negatively regulates the activation of SMAD and ERK pathways.

Next, we tested the role of miR-25–5p downregulation in the function of *Nell1*/EVs. As shown in Fig. 7E, when cells were pretransfected with miR-NC, the *Nell1*/EVs significantly upregulated the ratio of phosphorylated ERK1/2 to total ERK1/2, SMAD2 to ACTIN, and phosphorylated SMAD2 to ACTIN (Fig. 7E) in BMSCs. However, when BMSCs were pretransfected with miR-25–5p mimics, this difference was not noted. Meanwhile, when pretransfected with miR-NC, *Nell1*/EV-treated BMSCs showed a marked increase in the protein level of osteogenic markers, OSX, Collagen I, and OPN. No significant difference in the expression of these osteogenic proteins was found between *Nell1*/EVs and *Ctrl*/EVs groups when cells were pretransfected with miR-25–5p mimics (Fig. 7E). Moreover, the level of ALP activity and mineralized nodules of BMSCs (with miR-NC pretransfection) treated by *Nell1*/EVs was significantly greater than that in *Ctrl*/EVs group, but it was reduced when pretransfected with miR-25–5p mimics (Fig. 7F). These results suggested that miR-25–5p/SMAD2/ERK is the critical mechanistic link required for the *Nell1*/EV-induced osteogenic differentiation.

3.6. Characterization of the 3D-EV-hydrogel system

To obtain EV delivery carriers for implantation at bone defect sites, a hydrogel system containing EVs was fabricated (Fig. 8A). *Ctrl*/EVs and *Nell1*/EVs were labeled with PKH67 and PKH26, respectively; then, they were incorporated into the hydrogel. The PBS-loaded hydrogel was used as a negative control. As shown in the fluorescence microscope image, *Ctrl*/EVs (green dots) and *Nell1*/EVs (red dots) were homogeneously distributed in the hydrogel, whereas there were few fluorescent dots in the PBS-loaded hydrogels (Fig. 8B). Furthermore, scanning electron microscopy images showed that the *Ctrl*/EVs and *Nell1*/EVs were incorporated into the hydrogel (Fig. 8C). These results demonstrated that 3D-EV-hydrogel system was built successfully.

Further studies on the weight remaining ratio of the hydrogels in doubly distilled water (DDW) at 37 °C were conducted. For the 3D-EV-hydrogel in DDW, the weight nearly remained unchanged during the first 4 days. A considerable decrease was observed between day 4 and day 8; then, the weight remainingslowly decreased to near zero over approximately one month (Fig. 8D). Moreover, the 3D-EV-hydrogel showed an initial (first 6–8 days) relatively rapid delivery of EVs followed by a more sustained and continuing release for up to 16 days (Fig. 8E).

To further demonstrate the advantage of using the hydrogel system to deliver EVs, the EVs retention ability was investigated *in vivo*. In experiment group, the 3D-EV-hydrogel was implanted into the bone defects directly. Control groups received an equal volume of EV suspension injections into the tail vein or directly into bone defects. As shown in Fig. 8F, the hydrogel system demonstrated the possibility for high doses of EVs (fluorescence-labeled) to exert therapeutic effects in calvarial defect in situ, and excellent fluorescence signal was still observed in the EV-hydrogel system after 9 days of implantation. However, even after 24 h, there were few EVs were observed at calvarial defect area in tail vein and local injection groups. These results showed that the 3D-EV-hydrogel could drastically improve EV retention rate *in vivo*.

3.7. Acellular hydrogel encasing Nell1/EVs induced bone tissue regeneration in vivo

Our findings revealed the highest level of tissue regeneration in the *Nell1*/EV-hydrogel group. Notably, the amount of newly formed bone in the *Nell1*/EV-hydrogel group was significantly greater than that in the *Ctrl*/EV-hydrogel, EV-free hydrogel, and control groups at an advanced stage (8 weeks, Fig. 9). Although the effects were less pronounced in the early stages (4 weeks, Fig. S5). The 3D sectional micro-computed tomography (micro-CT) images showed reconstruction of anatomical structure of skull in the three groups (Fig. 9A). Quantitative micro-CT analysis (Fig. 9B–F) revealed that the bone volume/tissue volume (BV/TV) of the *Nell1*/EV-hydrogel group (26.14% ± 4.42%) was significantly higher than that of the *Ctrl*/EV-Hydrogel group (23.94% ± 7.23%). The hydrogel group (19.06% ± 5.61%) performed poorly, with a BV/TV lower than that in the Control group (23.93% ± 5.85%). Bone mineral density (BMD), bone surface density (BS/TV), and trabecular thickness (Tb. Th) showed a similar trend; that was, the group treated with *Nell1*/EV-hydrogel showed significantly better bone regeneration than the control group.

Consistent with the micro-CT findings, hematoxylin and eosin (H&E) staining revealed that new bone formation in the defect area was markedly increased in the *Nell1*/EV-hydrogel group, whereas only a small amount of new bone formation was detected in the *Ctrl*/EV-hydrogel and hydrogel without EVs (Fig. 9G). Masson trichrome staining revealed that the cortical bone in the *Nell1*/EV-hydrogel group was almost completely regenerated (Fig. 9H). Moreover, immunostaining revealed that the expression of osteoblast differentiation markers, including NELL1 and OCN, was increased in the *Nell1*/EV-hydrogel group when compared with *Ctrl*/EV-hydrogel and hydrogel without EVs (Fig. 9I-L). The total NELL1-positive and OCN-positive areas differed among the *Nell1*/EV-hydrogel group and remaining groups, indicating the promotion of bone regeneration in this group. These results suggest that the hydrogel assembled with *Nell1*/EVs can induce new bone formation *in vivo*.

4. Discussion

BMSC-EVs are useful in bone regeneration for overcoming issues such as inflammation, lower seeding efficiency, and immune response of cell transplantation, as well as enabling fast release and rapid concentration decay of growth factors [50,52,53]. Based on our previous findings [46], we further investigated the osteogenic capacity of EVs derived from *Nell1*-modified BMSCs and determined how *Nell1*-induced differentiation was coordinated with EV-miRNA changes. We isolated EVs from *Nell1*-modified BMSCs and demonstrated that modified EVs were able to induce BMSC osteogenesis *in vitro* and repaired bone defects *in vivo*. Our results indicate the following: (a) as an acellular strategy for bone tissue regeneration, *Nell1*/EVs significantly promoted BMSC proliferation and osteogenic differentiation *in vitro* and *in vivo*; (b) the expression profile of miRNAs in BMSC-EVs was altered by *Nell1* modification; and (c) the beneficial effect of *Nell1*/EVs is related to miR-25–5p and its downstream SMAD2 and ERK pathways (Fig. 10).

When the expression of osteogenesis-related genes is altered, cells undergo many molecular and subsequent EV cargo changes, which may further affect intercellular communication and change osteogenic

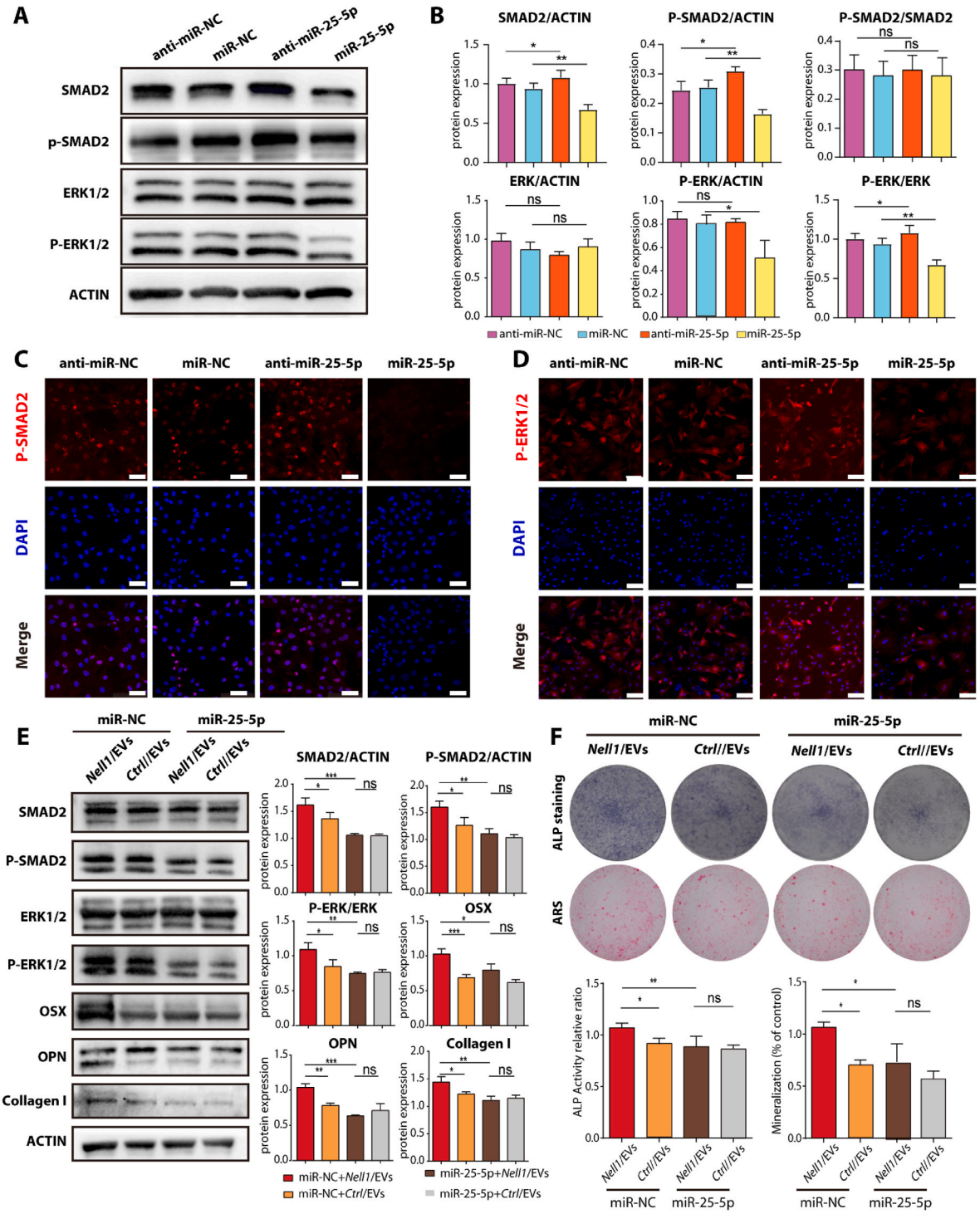

Fig. 7. miR-25-5p/SMAD2/ERK as the critical mechanistic link required for the osteogenic capacity of Nell1/EVs. (A and B) Representative immunoblots and quantification of Western blot analysis of SMAD2, *p*-SMAD2, ERK1/2, and *p*-ERK1/2 protein. **(C)** *p*-SMAD2 and **(D)** *p*-ERK1/2 levels were analyzed by confocal immunofluorescence microscopy. Scale bars: 100 μm. **(E)** Representative immunoblots and quantification analysis of Western blot analysis of SMAD2, *p*-SMAD2, ERK1/2, and *p*-ERK1/2 protein, and osteogenic markers: Osterix (Osx), Osteopontin (OPN), and Collagen I. **(F)** ALP and Alizarin red staining, quantitative ALP assay, and semi-quantification of mineralized nodules at 14 days post-transfection. *$p < 0.05$, **$p < 0.01$, via one-way analysis of variance, n = 3. MiR-25–5p, miR-25–5p mimics; anti-miR-25–5p, miR-25–5p inhibitors; miR-NC, mimic negative control; anti-miR-NC, inhibitor negative control. MiR-NC + Nell1/EVs: transfected with negative control mimics before treatment with Nell1/EVs; miR-NC + Ctrl/EVs: transfected with negative control mimics before treatment with Ctrl/EVs; miR-25–5p + Nell1/EVs: transfected with miR-25–5p mimics before treatment with Nell1/EVs; miR-25–5p + Ctrl/EVs: transfected with miR-25–5p mimics before treatment with Ctrl/EVs. One-way analysis of variance was used. *$p < 0.05$, **$p < 0.01$, ***$p < 0.001$, NS, non-significant, n = 3.

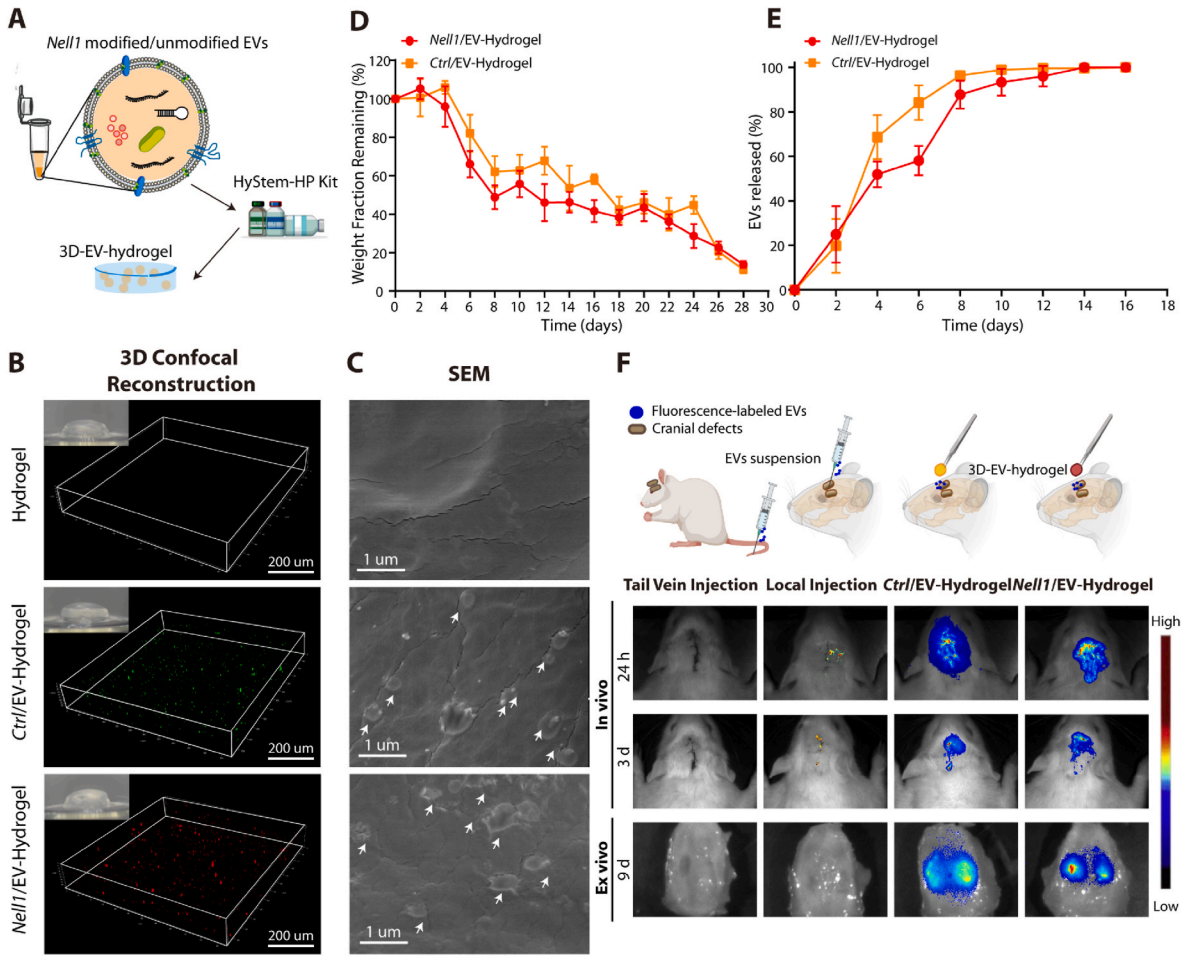

Fig. 8. Construction and characterization of the EV-hydrogel system. (A) Schematic representation of the EV-loaded hydrogel. **(B)** Distribution of PKH67-labeled *Ctrl*/EVs in the hydrogel and PKH26-labeled *Nell1*/EVs in the hydrogel; hydrogel without EVs was used as a negative control. **(C)** Scanning electron microscopy (SEM) images of the 3D-EV-hydrogel system. *Ctrl*/EVs and *Nell1*/EVs were incorporated into the hydrogels. White arrows indicate *Ctrl*/EVs and *Nell1*/EVs. **(D)** Weight loss of the *Ctrl*/EV-hydrogel and *Nell1*/EV-hydrogel in doubly distilled water as a function of time. **(E)** *Ctrl*/EVs and *Nell1*/EVs release profile from the hydrogels. **(F)** *In vivo* or *ex vivo* fluorescence imaging of EVs suspension (EVs in PBS) and in the 3D hydrogel. All groups of EVs were labeled using a near infrared (NIR) fluorescent labeling agent before implantation. Schematic picture was created with BioRender.

microenvironment. In this study, BMSCs were selected to investigate the *Nell1*-mediated osteogenic impact, as EVs are prone to be captured by cells from the same lineage as producer cells. Our data revealed that secretion contributed to the *Nell1* osteogenic therapeutic effects, which were compromised after inhibiting the secretion of EVs. To the best of our knowledge, this study is the first to demonstrate that *Nell1* impacts bone tissue repair relying on EV-associated intercellular communication. Unexpectedly, the NELL1 protein, enriched in *Nell1*/BMSCs, was not sorted into *Nell1*/EVs (Fig. 3C). These results demonstrate that although NELL1 protein was overexpressed in BMSCs, the corresponding EVs do not contain NELL1 protein as an EV content. Consistent with our research, studies revealed that even though BMP2 was overexpressed in MSCs, the functionally engineered EVs do not contain BMP2 protein. Further investigations revealed that EVs derived from BMP2 -overexpressed MSCs potentiate the BMP2 signaling cascade, possibly due to an altered miRNA composition [35].

The modes of EVs interaction with target cells have described two possible ways: cargo delivery and activation of surface receptors and signaling [54]. Both these two modes are present at 37 °C; but when the temperature decreases to 4 °C, cargo delivery is suppressed due to endocytosis limitations [55,56]. In the present study, few labeled EVs were observed to bind to BMSCs when cocultured at 4 °C by confocal microscopy imaging, which demonstrated that *Nell1*/EVs exerted the pro-osteogenic effect through cargo delivery than surface binding. Furthermore, we found that the *Nell1* modification of BMSCs affects their miRNA secretion through EVs, thereby examining the miRNA profile of *Nell1*/EVs and *Ctrl*/EVs. The miRNA profile of *Nell1*/EVs significantly differed from that of *Ctrl*/EVs. This result is similar to an earlier finding, in which the miRNA expression profile is radically altered in response to BMP2 induction [57]. Moreover, the miRNA profiles indicated that the altered miRNAs in the *Nell1*/EV group regulated aging, ERK1/ERK2 cascade, angiogenesis, TGF-β, and BMP signaling pathways (Fig. 5). These classical signaling pathways have been shown to drive the osteogenic differentiation of stem cells [58–60]. Our results demonstrate that *Nell1* regulates BMSC osteogenesis via selective regulation of osteogenic miRNA in EVs.

Through bio-information analysis and biological verification tests, we screened miR-25–5p and confirmed the important role of the miR-25–5p/SMAD2 signaling axis in osteogenesis induced by *Nell1*. These findings provide insights into the intricate mechanisms of *Nell1* in bone formation. Previous studies showed that *Nell1* functions through activating of ERK, JNK, MAPK, and Wnt/β-catenin pathways [59,60], but TGF-β/Smad signaling or p38 were not elucidated related [61]. However, we demonstrated that *Nell1*/EVs regulated osteogenesis through the TGF-β/Smad pathway. Activated receptor-regulated SMADs, including SMAD 1, 2, 3, 5, and 8, act as critical intracellular receptors and intermediaries of the canonical TGF-β and BMP superfamily pathways [62]. In the present study, SMAD2 (a key transcription factor

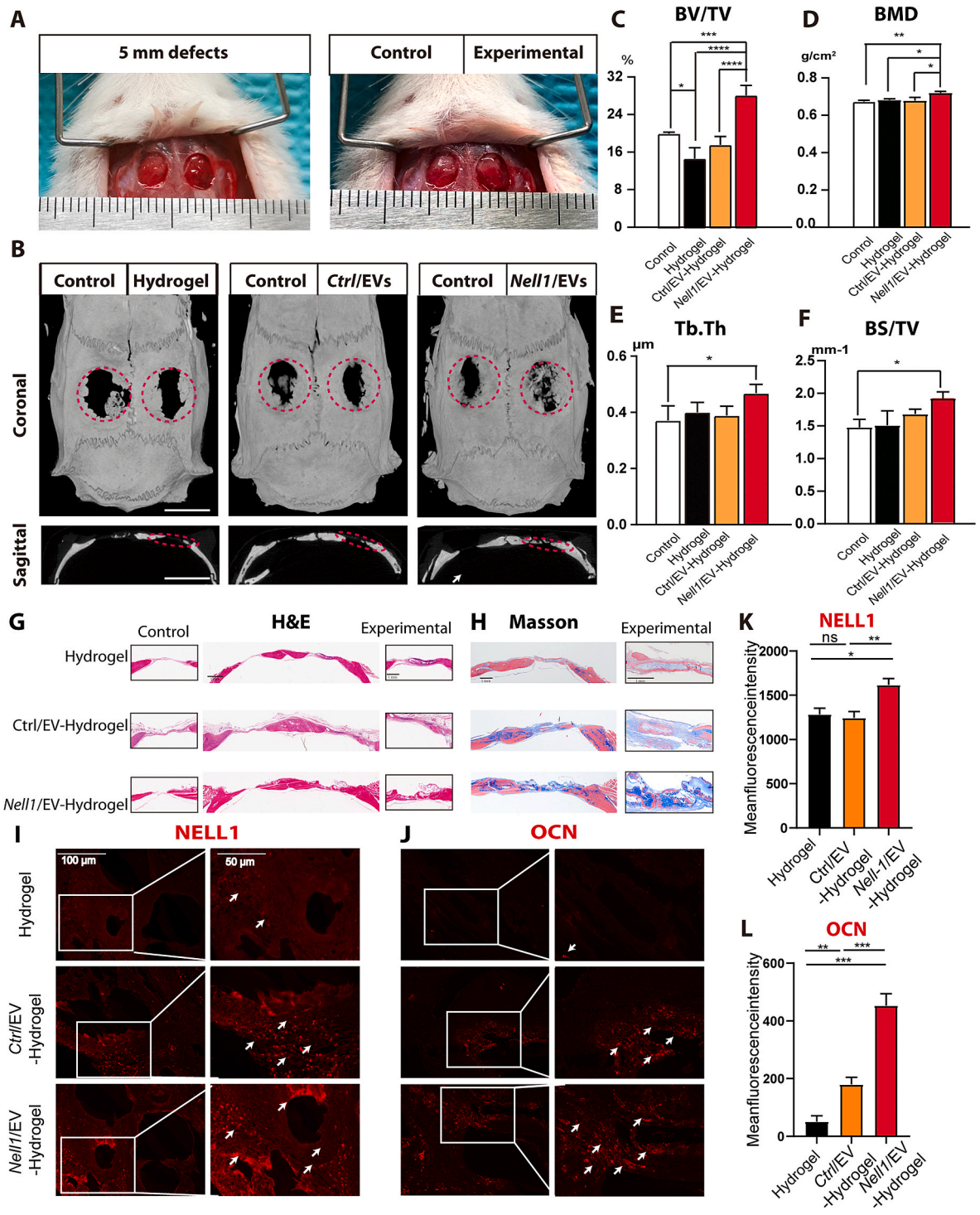

Fig. 9. Building an acellular hydrogel encasing *Nell1*/EVs to repair rat calvarial defects. (A) Two circular critical-sized calvarial defects (diameter, 5 mm) were created. The defects on the left side were untreated as a control. The defects on the right side were treated with either hydrogel without EVs or hydrogel loaded with *Ctrl*/EVs or *Nell1*/EVs. **(B)** 3D reconstruction images were obtained postoperatively. Scale bars: 5 mm. Analysis of **(C)** Bone volume/tissue volume (BV/TV), **(D)** Bone mineral density (BMD), **(E)** Trabecular thickness (Tb. Th) and **(F)** Bone surface density (BS/TV) in each group. **(G)** H&E staining of decalcified sections from each group. **(H)** Masson trichrome staining of decalcified sections; newly formed bone is shown in blue. Immunofluorescence for **(I)** NELL1 and **(J)** OCN in each group, where arrows indicate NELL1-positive or OCN-positive cell. Scale bar: 100 μm. **(K)** and **(L)** Quantitative immunofluorescence analysis. *$p < 0.05$, **$p < 0.01$, ***$p < 0.001$, ****$p < 0.0001$, NS, non-significant, using one-way analysis of variance, $n = 6$.

activated by TGF-β receptors) was identified as a direct and functional target of miR-25–5p through miRNA-targeting prediction and identification. After overexpression of miR-25–5p in BMSCs, SMAD2 expression was inhibited via direct binding of miR-25–5p to the 3'-UTR of SMAD2. Thus, mRNA and protein expression of SMAD2 was determined. Since, SMAD2 is not involved in BMP signaling [63,64], we also did not observe that *Nell1* could affect the BMP pathway through EV-mediated paracrine signaling [44,61]. Liu et al. also confirmed that the TGF-β/SMAD pathway played a critical role in bone repair by regulating BMSC-osteoinductive-EVs recently [65]. Moreover, we demonstrated

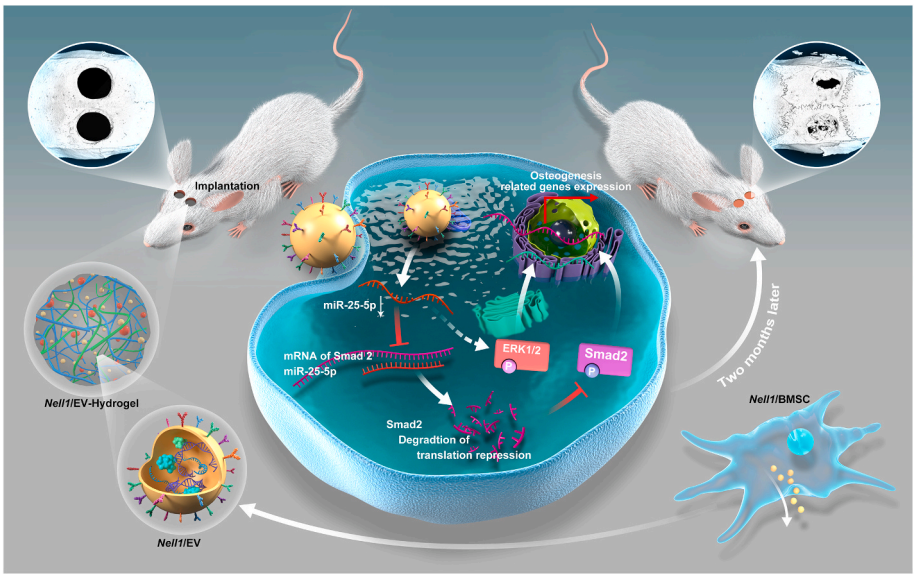

Fig. 10. *Nell1*/EV encasing acellular hydrogel sustained-release systems stimulate better bone formation in calvarial defects of rats. The miR-25–5p/SMAD2 signaling axis and ERK pathway play a role in modulating *Nell1*-induced osteogenic differentiation.

that miR-25–5p inhibited the SMAD pathway in BMSCs, which was in parallel with the ERK1/2 cascade (Fig. 7). Crosstalk between these two pathways has been reported previously [66], and their activation can synergistically promote osteogenesis [67]. In this study, we determined a novel regulatory mechanism by which *Nell1* induces osteogenesis. *Nell1* can affect paracrine signaling by affecting the levels of regulatory miRNAs in EVs and activating the SMAD and ERK signaling pathways.

The potential of employing EVs as an alternative acellular approach to cell therapy has attracted wide attention for repairing bone defects. However, the stability and retention of EVs are main limitations to their clinical translation, as they are rapidly cleared by the innate immune system [68]. EVs are rapidly sequestered and cleared when administered via bolus injections [69] and may cause unanticipated side effects by encasing various bioactive factors in unintended areas. Bone regeneration is a well-orchestrated process with a specific timeframe. It is favored that the bioactive substances are slowly and continuously released. Regarding the implanted materials, they can dissolve over the course of bone regeneration while providing mechanical support [70]. Biomaterials can overcome the low tissue retention associated with bolus EV injections and offer a controlled release platform for healing tissues [71–73]. Therefore, after the 3D-EV-hydrogel system was established, we demonstrated that the EVs were released over 16 days (Fig. 8E), and the duration of release and EV-hydrogel degradation were well synchronized (Fig. 8D). More importantly, when compared with EVs administered via the tail vein and local injection, the 3D-EV-hydrogel system was able to sustain a much higher EV concentrations in bone defect area, thereby considerably reducing the total required EVs (Fig. 8F). As a result, the computational costs were also greatly reduced. Collectively, these results indicated that the 3D-EV-hydrogel system could support bone regeneration, while providing mechanical strength and releasing the EVs in a sustained mode over a prolonged period.

EVs derived from *Nell1*/BMSCs can be easily encapsulated in 3D hydrogel scaffolds. After transplantation, modified EVs release various molecules (here, we focused on miRNAs) into the microenvironment to mobilize cells, thereby facilitating tissue remodeling [74–76]. Compared to *Ctrl*/EV-hydrogel and EV-free hydrogel scaffolds, *Nell1*/EV-hydrogel scaffolds improved the efficacy of acellular bone regenerative therapies. The healing patterns revealed that-rather than healing from the center of the defect-the bone defects were filled with new bone growing from the edge of the parietal bone plates. This result suggests that *Nell1*/EVs initiate the process of intramembranous bone regeneration by BMSCs that are present at the edge of the bone defect. Such a cell-free EV modification strategy circumvents the immune rejection caused by the transplantation of foreign cells. Compared to cellular therapy, it is straight-forward and provides extended stability in bone defects [27,77]. In this study, the Ctrl/EV-Hydrogel group did not exhibit significant difference with Hydrogel group at 8 weeks. This agrees with the results of another research that showed no difference in bone volume/tissue volume between Control EV and Collagen Control groups at 8 weeks; however, the difference between both groups became significant at 12 weeks [35]. In both studies, this delayed osteogenic capacity may partly due to a potential negative side-effects of viral transduction of host cells. In our study, the *Nell1*/EV-hydrogel group presented significantly enhanced osteogenic properties compared to the other two groups at 8 weeks. Thus, we will further study the effect of *Ctrl*/EV-Hydrogel with more extended observation in future research. Overall, this study provides insights into the osteoinductive effect of *Nell1* and reveals a promising strategy that can be used in regenerative medicine and tissue engineering for bone repair.

5. Conclusion

Therapeutic strategies based on EVs derived from *Nell1*-modified BMSCs (*Nell1*/EVs) were developed to improve the bone repair process *in vitro* and *in vivo*. We demonstrated that *Nell1*/EVs can effectively induce the osteogenic differentiation of BMSCs, and a decrease in miR-25–5p contributed to *Nell1*-induced osteogenesis by targeting the *Smad2* gene and mediating SMAD and ERK pathway. A 3D-EV-hydrogel with *Nell1*/EVs was established and achieved acellular bone regeneration within 8 weeks. Hence, our results show that *Nell1*/EVs can be used to replace stem cells in bone regeneration thereby providing novel understanding toward how *Nell1* mediate cell fate decisions of stem cells, through EVs.

Ethics statement

The *in vivo* study was approved by the Ethics Committee for Animal Research at Zhejiang University (ethics approval number: ZJU20200075). All procedures were conducted in accordance with the Declaration of Helsinki and standard guidelines.

Funding

This work was jointly supported by the National Natural Science Foundation of China, China (grant nos. 81771118).

Availability of data and materials

The datasets used and/or analyzed during the current study are available from the corresponding author on reasonable request.

Declaration of competing interest

No relevant conflicts of interest to declare.

CRediT authorship contribution statement

Yanhua Lan: Conceptualization, Writing – original draft, Investigation. **Huizhi Xie:** Conceptualization, Writing – original draft, Investigation. **Qianrui Jin:** Investigation. **Xiaomin Zhao:** Visualization. **Yang Shi:** Investigation. **Yanyan Zhou:** Investigation. **Zihe Hu:** Data curation. **Yi Ye:** Formal analysis. **Xiaoyuan Huang:** Investigation. **Yingjia Sun:** Formal analysis. **Zhuo Chen:** Project administration, Supervision, Writing – review & editing. **Zhijian Xie:** Project administration, Supervision, Writing – review & editing.

Acknowledgements

The authors thank Jue Shi, the surgeon of Stomatology Hospital, School of Stomatology, Zhejiang University School of Medicine, China, for her support during the design and revision of the manuscript.

Appendix A. Supplementary data

Supplementary data to this article can be found online at https://doi.org/10.1016/j.bioactmat.2022.01.019.

References

[1] S. Lin, G. Yang, F. Jiang, M. Zhou, S. Yin, Y. Tang, T. Tang, Z. Zhang, W. Zhang, X. Jiang, A magnesium-enriched 3D culture system that mimics the bone development microenvironment for vascularized bone regeneration, Adv. Sci. 6 (12) (2019) 1900209.

[2] K. Shimizu, A. Ito, H. Honda, Mag-seeding of rat bone marrow stromal cells into porous hydroxyapatite scaffolds for bone tissue engineering, J. Biosci. Bioeng. 104 (3) (2007) 171–177.

[3] T. Zhang, Q. Wei, H. Zhou, Z. Jing, X. Liu, Y. Zheng, H. Cai, F. Wei, L. Jiang, M. Yu, Y. Cheng, D. Fan, W. Zhou, X. Lin, H. Leng, J. Li, X. Li, C. Wang, Y. Tian, Z. Liu, Three-dimensional-printed individualized porous implants: a new "implant-bone" interface fusion concept for large bone defect treatment, Bioact Mater 6 (11) (2021) 3659–3670.

[4] M. Riazifar, E.J. Pone, J. Lötvall, W. Zhao, Stem cell extracellular vesicles: extended messages of regeneration, Annu. Rev. Pharmacol. Toxicol. 57 (2017) 125–154.

[5] Z. Chen, C. Wu, W. Gu, T. Klein, R. Crawford, Y. Xiao, Osteogenic differentiation of bone marrow MSCs by β-tricalcium phosphate stimulating macrophages via BMP2 signalling pathway, Biomaterials 35 (5) (2014) 1507–1518.

[6] M.P. Nikolova, M.S. Chavali, Recent advances in biomaterials for 3D scaffolds: a review, Bioact Mater 4 (2019) 271–292.

[7] Z. Qiao, M. Lian, Y. Han, B. Sun, X. Zhang, W. Jiang, H. Li, Y. Hao, K. Dai, Bioinspired stratified electrowritten fiber-reinforced hydrogel constructs with layer-specific induction capacity for functional osteochondral regeneration, Biomaterials 266 (2021), 120385.

[8] Y. Feng, Z. Jiang, Y. Zhang, X. Miao, Q. Yu, Z. Xie, G. Yang, Stem-cell-derived ECM sheet-implant complexes for enhancing osseointegration, Biomater Sci 8 (23) (2020) 6647–6656.

[9] F. Shang, Y. Yu, S. Liu, L. Ming, Y. Zhang, Z. Zhou, J. Zhao, Y. Jin, Advancing application of mesenchymal stem cell-based bone tissue regeneration, Bioact Mater 6 (3) (2021) 666–683.

[10] C. Maniatopoulos, J. Sodek, A.H. Melcher, Bone formation in vitro by stromal cells obtained from bone marrow of young adult rats, Cell Tissue Res. 254 (2) (1988) 317–330.

[11] S. Bian, L. Zhang, L. Duan, X. Wang, Y. Min, H. Yu, Extracellular vesicles derived from human bone marrow mesenchymal stem cells promote angiogenesis in a rat myocardial infarction model, J. Mol. Med. (Berl.) 92 (4) (2014) 387–397.

[12] Y. Shi, G. Hu, J. Su, W. Li, Q. Chen, P. Shou, C. Xu, X. Chen, Y. Huang, Z. Zhu, X. Huang, X. Han, N. Xie, G. Ren, Mesenchymal stem cells: a new strategy for immunosuppression and tissue repair, Cell Res. 20 (5) (2010) 510–518.

[13] T. Zhao, Z.N. Zhang, Z. Rong, Y. Xu, Immunogenicity of induced pluripotent stem cells, Nature 474 (7350) (2011) 212–215.

[14] M.F. Pittenger, A.M. Mackay, S.C. Beck, R.K. Jaiswal, R. Douglas, J.D. Mosca, M. A. Moorman, D.W. Simonetti, S. Craig, D.R. Marshak, Multilineage potential of adult human mesenchymal stem cells, Science 284 (5411) (1999) 143–147.

[15] B. Sui, C. Hu, L. Liao, Y. Chen, X. Zhang, X. Fu, C. Zheng, M. Li, L. Wu, X. Zhao, Y. Jin, Mesenchymal progenitors in osteopenias of diverse pathologies: differential characteristics in the common shift from osteoblastogenesis to adipogenesis, Sci. Rep. 6 (2016) 30186.

[16] M. Gnecchi, H. He, O.D. Liang, L.G. Melo, F. Morello, H. Mu, N. Noiseux, L. Zhang, R.E. Pratt, J.S. Ingwall, V.J. Dzau, Paracrine action accounts for marked protection of ischemic heart by Akt-modified mesenchymal stem cells, Nat. Med. 11 (4) (2005) 367–368.

[17] H. Xin, Y. Li, Z. Liu, X. Wang, X. Shang, Y. Cui, Z.G. Zhang, M. Chopp, MiR-133b promotes neural plasticity and functional recovery after treatment of stroke with multipotent mesenchymal stromal cells in rats via transfer of exosome-enriched extracellular particles, Stem Cell. 31 (12) (2013) 2737–2746.

[18] S. Cosenza, M. Ruiz, K. Toupet, C. Jorgensen, D. Noël, Mesenchymal stem cells derived exosomes and microparticles protect cartilage and bone from degradation in osteoarthritis, Sci. Rep. 7 (1) (2017), 16214.

[19] M. Brennan, P. Layrolle, D.J. Mooney, Biomaterials functionalized with MSC secreted extracellular vesicles and soluble factors for tissue regeneration, Adv. Funct. Mater. 30 (37) (2020).

[20] F. Diomede, M. D'Aurora, A. Gugliandolo, I. Merciaro, T. Orsini, V. Gatta, A. Piattelli, O. Trubiani, E. Mazzon, Biofunctionalized scaffold in bone tissue repair, Int. J. Mol. Sci. 19 (4) (2018).

[21] S. Zhang, S.J. Chuah, R.C. Lai, J.H.P. Hui, S.K. Lim, W.S. Toh, MSC exosomes mediate cartilage repair by enhancing proliferation, attenuating apoptosis and modulating immune reactivity, Biomaterials 156 (2018) 16–27.

[22] M.R. Puno, E.M. Weick, M. Das, C.D. Lima, SnapShot: the RNA exosome, Cell 179 (1) (2019), 282-282.e1.

[23] D.G. Phinney, M.F. Pittenger, Concise review: MSC-derived exosomes for cell-free therapy, Stem Cell. 35 (4) (2017) 851–858.

[24] D.G. Phinney, M. Di Giuseppe, J. Njah, E. Sala, S. Shiva, C.M. St Croix, D.B. Stolz, S. C. Watkins, Y.P. Di, G.D. Leikauf, J. Kolls, D.W. Riches, G. Deiuliis, N. Kaminski, S. V. Boregowda, D.H. McKenna, L.A. Ortiz, Mesenchymal stem cells use extracellular vesicles to outsource mitophagy and shuttle microRNAs, Nat. Commun. 6 (2015) 8472.

[25] H. Valadi, K. Ekström, A. Bossios, M. Sjöstrand, J.J. Lee, J.O. Lötvall, Exosome-mediated transfer of mRNAs and microRNAs is a novel mechanism of genetic exchange between cells, Nat. Cell Biol. 9 (6) (2007) 654–659.

[26] F. Liu, S. Hu, H. Yang, Z. Li, K. Huang, T. Su, S. Wang, K. Cheng, Hyaluronic acid hydrogel integrated with mesenchymal stem cell-secretome to treat endometrial injury in a rat model of Asherman's syndrome, Adv. Healthc. Mater. 8 (14) (2019), e1900411.

[27] M. Liang, W. Liu, Z. Peng, S. Lv, Y. Guan, G. An, Y. Zhang, T. Huang, Y. Wang, The therapeutic effect of secretome from human umbilical cord-derived mesenchymal stem cells in age-related osteoporosis, Artif. Cells Nanomed. Biotechnol. 47 (1) (2019) 1357–1366.

[28] J. Phan, P. Kumar, D. Hao, K. Gao, D. Farmer, A. Wang, Engineering mesenchymal stem cells to improve their exosome efficacy and yield for cell-free therapy, J. Extracell. Vesicles 7 (1) (2018) 1522236.

[29] A. Tieu, M.M. Lalu, M. Slobodian, C. Gnyra, D.A. Fergusson, J. Montroy, D. Burger, D.J. Stewart, D.S. Allan, An analysis of mesenchymal stem cell-derived extracellular vesicles for preclinical use, ACS Nano 14 (8) (2020) 9728–9743.

[30] Y. Cao, T. Wu, K. Zhang, X. Meng, W. Dai, D. Wang, H. Dong, X. Zhang, Engineered exosome-mediated near-infrared-II region V(2)C quantum dot delivery for nucleus-target low-temperature photothermal therapy, ACS Nano 13 (2) (2019) 1499–1510.

[31] C. Feng, Z. Xiong, C. Wang, W. Xiao, H. Xiao, K. Xie, K. Chen, H. Liang, X. Zhang, H. Yang, Folic acid-modified Exosome-PH20 enhances the efficiency of therapy via modulation of the tumor microenvironment and directly inhibits tumor cell metastasis, Bioact Mater 6 (4) (2021) 963–974.

[32] I.K. Herrmann, M.J.A. Wood, G. Fuhrmann, Extracellular vesicles as a next-generation drug delivery platform, Nat. Nanotechnol. 16 (7) (2021) 748–759.

[33] P. Wu, B. Zhang, D.K.W. Ocansey, W. Xu, H. Qian, Extracellular vesicles: a bright star of nanomedicine, Biomaterials 269 (2021), 120467.

[34] C.H. Lu, Y.A. Chen, C.C. Ke, R.S. Liu, Mesenchymal stem cell-derived extracellular vesicle: a promising alternative therapy for osteoporosis, Int. J. Mol. Sci. 22 (23) (2021).

[35] C.C. Huang, M. Kang, Y. Lu, S. Shirazi, J.I. Diaz, L.F. Cooper, P. Gajendrareddy, S. Ravindran, Functionally engineered extracellular vesicles improve bone regeneration, Acta Biomater. 109 (2020) 182–194.

[36] H. Li, D. Liu, C. Li, S. Zhou, D. Tian, D. Xiao, H. Zhang, F. Gao, J. Huang, Exosomes secreted from mutant-HIF-1α-modified bone-marrow-derived mesenchymal stem cells attenuate early steroid-induced avascular necrosis of femoral head in rabbit, Cell Biol. Int. 41 (12) (2017) 1379–1390.

[37] B. Huang, Y. Su, E. Shen, M. Song, D. Liu, H. Qi, Extracellular vesicles from GPNMB-modified bone marrow mesenchymal stem cells attenuate bone loss in an ovariectomized rat model, Life Sci. (272) (2021), 119208.

[38] K. Zhang, X. Zhao, X. Chen, Y. Wei, W. Du, Y. Wang, L. Liu, W. Zhao, Z. Han, D. Kong, Q. Zhao, Z. Guo, Z. Han, N. Liu, F. Ma, Z. Li, Enhanced therapeutic effects of mesenchymal stem cell-derived exosomes with an injectable hydrogel for

hindlimb ischemia treatment, ACS Appl. Mater. Interfaces 10 (36) (2018) 30081–30091.
[39] S. Mardpour, M.H. Ghanian, H. Sadeghi-Abandansari, S. Mardpour, A. Nazari, F. Shekari, H. Baharvand, Hydrogel-mediated sustained systemic delivery of mesenchymal stem cell-derived extracellular vesicles improves hepatic regeneration in chronic liver failure, ACS Appl. Mater. Interfaces 11 (41) (2019) 37421–37433.
[40] J. Pizzicannella, F. Diomede, A. Gugliandolo, L. Chiricosta, P. Bramanti, I. Merciaro, T. Orsini, E. Mazzon, O. Trubiani, 3D printing PLA/gingival stem cells/EVs upregulate miR-2861 and -210 during osteoangiogenesis commitment, Int. J. Mol. Sci. 20 (13) (2019).
[41] H. Hu, L. Dong, Z. Bu, Y. Shen, J. Luo, H. Zhang, S. Zhao, F. Lv, Z. Liu, miR-23a-3p-abundant small extracellular vesicles released from Gelma/nanoclay hydrogel for cartilage regeneration, J. Extracell. Vesicles 9 (1) (2020), 1778883.
[42] A.W. James, J. Shen, X. Zhang, G. Asatrian, R. Goyal, J.H. Kwak, L. Jiang, B. Bengs, C.T. Culiat, A.S. Turner, H.B. Seim Iii, B.M. Wu, K. Lyons, J.S. Adams, K. Ting, C. Soo, NELL-1 in the treatment of osteoporotic bone loss, Nat. Commun. 6 (2015) 7362.
[43] Y. Zhang, O. Velasco, X. Zhang, K. Ting, C. Soo, B.M. Wu, Bioactivity and circulation time of PEGylated NELL-1 in mice and the potential for osteoporosis therapy, Biomaterials 35 (24) (2014) 6614–6621.
[44] X. Zhang, J. Zara, R.K. Siu, K. Ting, C. Soo, The role of NELL-1, a growth factor associated with craniosynostosis, in promoting bone regeneration, J. Dent. Res. 89 (9) (2010) 865–878.
[45] C. Li, X. Zhang, Z. Zheng, A. Nguyen, K. Ting, C. Soo, Nell-1 is a key functional modulator in osteochondrogenesis and beyond, J. Dent. Res. 98 (13) (2019) 1458–1468.
[46] Y. Lan, Q. Jin, H. Xie, C. Yan, Y. Ye, X. Zhao, Z. Chen, Z. Xie, Exosomes enhance Adhesion and osteogenic differentiation of initial bone marrow stem cells on titanium surfaces, Front. Cell Dev. Biol. 8 (2020) 583234.
[47] C. Théry, S. Amigorena, G. Raposo, A. Clayton, Isolation and characterization of exosomes from cell culture supernatants and biological fluids, Curr. Protoc. Cell Biol. 30 (2006) 3.22.1–3.22.29.
[48] B.N. Davis, A.C. Hilyard, G. Lagna, A. Hata, SMAD proteins control DROSHA-mediated microRNA maturation, Nature 454 (7200) (2008) 56–61.
[49] F.M. Moussa, B.P. Cook, G.R. Sondag, M. DeSanto, M.S. Obri, S.E. McDermott, F. F. Safadi, The role of miR-150 regulates bone cell differentiation and function, Bone (145) (2021), 115470.
[50] T. Xu, Y. Luo, J. Wang, N. Zhang, C. Gu, L. Li, D. Qian, W. Cai, J. Fan, G. Yin, Exosomal miRNA-128-3p from mesenchymal stem cells of aged rats regulates osteogenesis and bone fracture healing by targeting Smad5, J. Nanobiotechnol. 18 (1) (2020) 47.
[51] S.R. Baglio, K. Rooijers, D. Koppers-Lalic, F.J. Verweij, M. Pérez Lanzón, N. Zini, B. Naaijkens, F. Perut, H.W. Niessen, N. Baldini, D.M. Pegtel, Human bone marrow- and adipose-mesenchymal stem cells secrete exosomes enriched in distinctive miRNA and tRNA species, Stem Cell Res. Ther. 6 (1) (2015) 127.
[52] A. Mokarizadeh, N. Delirezh, A. Morshedi, G. Mosayebi, A.A. Farshid, K. Mardani, Microvesicles derived from mesenchymal stem cells: potent organelles for induction of tolerogenic signaling, Immunol. Lett. 147 (1–2) (2012) 47–54.
[53] P.D. Robbins, A.E. Morelli, Regulation of immune responses by extracellular vesicles, Nat. Rev. Immunol. 14 (3) (2014) 195–208.
[54] G. van Niel, G. D'Angelo, G. Raposo, Shedding light on the cell biology of extracellular vesicles, Nat. Rev. Mol. Cell Biol. 19 (4) (2018) 213–228.
[55] G. Ahmadian, W. Ju, L. Liu, M. Wyszynski, S.H. Lee, A.W. Dunah, C. Taghibiglou, Y. Wang, J. Lu, T.P. Wong, M. Sheng, Y.T. Wang, Tyrosine phosphorylation of GluR2 is required for insulin-stimulated AMPA receptor endocytosis and LTD, EMBO J. 23 (5) (2004) 1040–1050.
[56] M. Son, A. Porat, M. He, J. Suurmond, F. Santiago-Schwarz, U. Andersson, T. R. Coleman, B.T. Volpe, K.J. Tracey, Y. Al-Abed, B. Diamond, C1q and HMGB1 reciprocally regulate human macrophage polarization, Blood 128 (18) (2016) 2218–2228.
[57] Z. Li, M.Q. Hassan, S. Volinia, A.J. van Wijnen, J.L. Stein, C.M. Croce, J.B. Lian, G. S. Stein, A microRNA signature for a BMP2-induced osteoblast lineage commitment program, Proc. Natl. Acad. Sci. U. S. A. 105 (37) (2008) 13906–13911.
[58] G. Chen, C. Deng, Y.P. Li, TGF-β and BMP signaling in osteoblast differentiation and bone formation, Int. J. Biol. Sci. 8 (2) (2012) 272–288.
[59] V.S. Salazar, L.W. Gamer, V. Rosen, BMP signalling in skeletal development, disease and repair, Nat. Rev. Endocrinol. 12 (4) (2016) 203–221.
[60] S. Zhang, K.Y.W. Teo, S.J. Chuah, R.C. Lai, S.K. Lim, W.S. Toh, MSC exosomes alleviate temporomandibular joint osteoarthritis by attenuating inflammation and restoring matrix homeostasis, Biomaterials 200 (2019) 35–47.
[61] N. Bokui, T. Otani, K. Igarashi, J. Kaku, M. Oda, T. Nagaoka, M. Seno, K. Tatematsu, T. Okajima, T. Matsuzaki, K. Ting, K. Tanizawa, S. Kuroda, Involvement of MAPK signaling molecules and Runx2 in the NELL1-induced osteoblastic differentiation, FEBS Lett. 582 (2) (2008) 365–371.
[62] C. Alarcón, A.I. Zaromytidou, Q. Xi, S. Gao, J. Yu, S. Fujisawa, A. Barlas, A. N. Miller, K. Manova-Todorova, M.J. Macias, G. Sapkota, D. Pan, J. Massagué, Nuclear CDKs drive Smad transcriptional activation and turnover in BMP and TGF-beta pathways, Cell 139 (4) (2009) 757–769.
[63] C.H. Heldin, K. Miyazono, P. ten Dijke, TGF-beta signalling from cell membrane to nucleus through SMAD proteins, Nature 390 (6659) (1997) 465–471.
[64] B. Levi, D.C. Wan, J.P. Glotzbach, J. Hyun, M. Januszyk, D. Montoro, M. Sorkin, A. W. James, E.R. Nelson, S. Li, N. Quarto, M. Lee, G.C. Gurtner, M.T. Longaker, CD105 protein depletion enhances human adipose-derived stromal cell osteogenesis through reduction of transforming growth factor β1 (TGF-β1) signaling, J. Biol. Chem. 286 (45) (2011) 39497–39509.
[65] A. Liu, D. Lin, H. Zhao, L. Chen, B. Cai, K. Lin, S.G. Shen, Optimized BMSC-derived osteoinductive exosomes immobilized in hierarchical scaffold via lyophilization for bone repair through Bmpr2/Acvr2b competitive receptor-activated Smad pathway, Biomaterials 272 (2021), 120718.
[66] R. Derynck, Y.E. Zhang, Smad-dependent and Smad-independent pathways in TGF-beta family signalling, Nature 425 (6958) (2003) 577–584.
[67] S.H. Hsu, G.S. Huang, Substrate-dependent Wnt signaling in MSC differentiation within biomaterial-derived 3D spheroids, Biomaterials 34 (20) (2013) 4725–4738.
[68] T. Imai, Y. Takahashi, M. Nishikawa, K. Kato, M. Morishita, T. Yamashita, A. Matsumoto, C. Charoenviriyakul, Y. Takakura, Macrophage-dependent clearance of systemically administered B16BL6-derived exosomes from the blood circulation in mice, J. Extracell. Vesicles 4 (2015), 26238.
[69] M. Zhai, Y. Zhu, M. Yang, C. Mao, Human mesenchymal stem cell derived exosomes enhance cell-free bone regeneration by altering their miRNAs profiles, Adv. Sci. 7 (19) (2020) 2001334.
[70] L.-B. Jiang, D.-H. Su, S.-L. Ding, Q.-C. Zhang, Z.-F. Li, F.-C. Chen, W. Ding, S.-T. Zhang, J. Dong, Salt-assisted toughening of protein hydrogel with controlled degradation for bone regeneration, Adv. Funct. Mater. 29 (26) (2019), 1901314.
[71] L. Liu, Y. Liu, C. Feng, J. Chang, R. Fu, T. Wu, F. Yu, X. Wang, L. Xia, C. Wu, B. Fang, Lithium-containing biomaterials stimulate bone marrow stromal cell-derived exosomal miR-130a secretion to promote angiogenesis, Biomaterials 192 (2019) 523–536.
[72] C. Wang, M. Wang, K. Xia, J. Wang, F. Cheng, K. Shi, L. Ying, C. Yu, H. Xu, S. Xiao, C. Liang, F. Li, B. Lei, Q. Chen, A bioactive injectable self-healing anti-inflammatory hydrogel with ultralong extracellular vesicles release synergistically enhances motor functional recovery of spinal cord injury, Bioact Mater 6 (8) (2021) 2523–2534.
[73] W. Li, Y. Liu, P. Zhang, Y. Tang, M. Zhou, W. Jiang, X. Zhang, G. Wu, Y. Zhou, Tissue-engineered bone immobilized with human adipose stem cells-derived exosomes promotes bone regeneration, ACS Appl. Mater. Interfaces 10 (6) (2018) 5240–5254.
[74] D. Zhang, H. Lee, Z. Zhu, J.K. Minhas, Y. Jin, Enrichment of selective miRNAs in exosomes and delivery of exosomal miRNAs in vitro and in vivo, Am. J. Physiol. Lung Cell Mol. Physiol. 312 (1) (2017) L110–l121.
[75] T.T. Tang, B. Wang, M. Wu, Z.L. Li, Y. Feng, J.Y. Cao, D. Yin, H. Liu, R.N. Tang, S. D. Crowley, L.L. Lv, B.C. Liu, Extracellular vesicle-encapsulated IL-10 as novel nanotherapeutics against ischemic AKI, Sci. Adv. 6 (33) (2020) eaaz0748.
[76] L.P. Zhu, T. Tian, J.Y. Wang, J.N. He, T. Chen, M. Pan, L. Xu, H.X. Zhang, X.T. Qiu, C.C. Li, K.K. Wang, H. Shen, G.G. Zhang, Y.P. Bai, Hypoxia-elicited mesenchymal stem cell-derived exosomes facilitates cardiac repair through miR-125b-mediated prevention of cell death in myocardial infarction, Theranostics 8 (22) (2018) 6163–6177.
[77] Y. Zha, Y. Li, T. Lin, J. Chen, S. Zhang, J. Wang, Progenitor cell-derived exosomes endowed with VEGF plasmids enhance osteogenic induction and vascular remodeling in large segmental bone defects, Theranostics 11 (1) (2021) 397–409.